EXPERIMENTAL STUDY ON OUT-OF-PLANE BEHAVIOR OF INFILL WALL BUILT IN RC FRAMES

Ho CHOI[1], Kazuto MATSUKAWA[2], Yasushi SANADA[3] and Yoshiaki NAKANO[4]

ABSTRACT: The objectives of this study are to investigate out-of-plane behavior of unreinforced masonry infills and to identify the effectiveness of the tie system, which was proposed to enhance the infill stability under both in- and out-of-plane forces. For this purpose, 1/4-scale, single-story, one-bay two masonry infilled RC frame specimens either with or without the proposed tie system applied to the infills, were tested under the in-plane static cyclic loading and out-of-plane dynamic excitation. In this paper, the seismic performance of both specimens under the in-plane static cyclic loading preliminarily performed before the dynamic excitation, and the maximum acceleration and displacement relations of both infills under the out-of-plane dynamic excitation were discussed. The damage to both infill walls after the in-plane and out-of-plane excitation was also compared.

Key Words: unreinforced masonry (URM) wall, tie system, reinforced concrete (RC) frame, out-of-plane behavior, shaking table test

INTRODUCTION

The authors have conducted the researches on in-plane seismic performance of reinforced concrete (RC) frames with unreinforced masonry (URM) wall, and found that URM infill walls improve in-plane seismic performance of overall frames (Jin, K. et al. (2016)). However, URM infill walls may fail in out-of-plane direction before their in-plane performance is fully exhibited, and such failure pattern was often found in the past earthquakes (e.g., the 1999 Taiwan Chi-Chi Earthquake, the 2003 Iran Bam Earthquake and the 2006 Indonesia Central Java Earthquake). Therefore, a reinforcing system to prevent out-of-plane failure is required to ensure the full contribution of the URM infills.

Under such background, a research project was initiated in collaboration between European and Japanese universities, under JST (Japan Science and Technology Agency) Concert-Japan (Connecting and Coordinating European Research and Technology Development with Japan) project. This project focused on a tie system, which was designed to ensure the infill stability under both in- and out-of-plane forces and to make a reliable contribution of the infill to the overall frame. Experimental and numerical studies were conducted by the Japanese and European teams, respectively, to validate and optimize the structural design methodology, as well as to develop the associated design procedures and guidelines.

In this study, the typical RC frames with infill walls in Turkey were experimentally investigated to confirm the out-of-plane behavior of the infills and to identify the effectiveness of the proposed tie

---

[1] Research Associate, Institute of Industrial Science, The University of Tokyo, Ph.D
[2] Research Associate, Institute of Industrial Science, The University of Tokyo, Ph.D
[3] Associate Professor, Graduate School of Engineering, Osaka University, Dr.Eng.
[4] Professor, Institute of Industrial Science, The University of Tokyo, Dr.Eng.

system under both in- and out-of-plane forces. In the experiments, 1/4-scale, single-story, one-bay two masonry infilled RC frame specimens either with or without the tie system applied to the infills, were tested under the in-plane static cyclic loading and out-of-plane dynamic excitation, respectively, and the acceleration and displacement of URM walls and overall frames were measured.

In this paper, the seismic performance of both specimens under the in-plane cyclic loading, preliminarily performed before the dynamic excitation, and the relationship between response acceleration and displacement of the overall frame under the dynamic excitation were discussed. In addition, the maximum acceleration and displacement relation of both infills, as well as the damage mitigation of infills due to the presence of the proposed tie system, were also investigated.

PROTOTYPE BUILDING AND SMALL SCALE SPECIMENS

In this study, a typical RC building in Turkey was selected as a reference building, and 1/4-scale models were prepared. Figure 1 shows the outlines of the reference building which has five stories with each story height of 3 meters and the plan dimensions of 23 meters by 16 meters. As shown in the figure, one-span of the interior frames in the longitudinal direction in the first story was focused to design the prototype frame. Two 1/4-scale specimens with one-story and one-bay were fabricated for this experimental study: One is the RC frame having an unreinforced masonry infill wall (URM wall specimen), and the other is the RC frame having a tie system in the infill wall (tie system specimen).
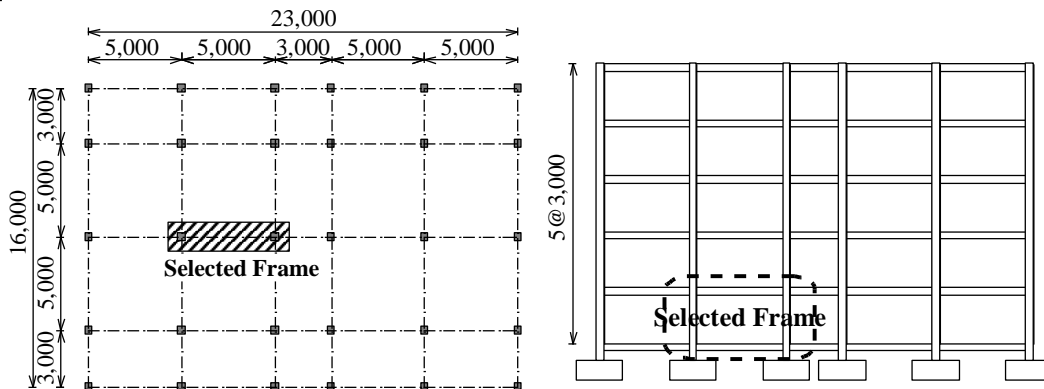
Figure 1. Outlines of the reference building (unit: mm)
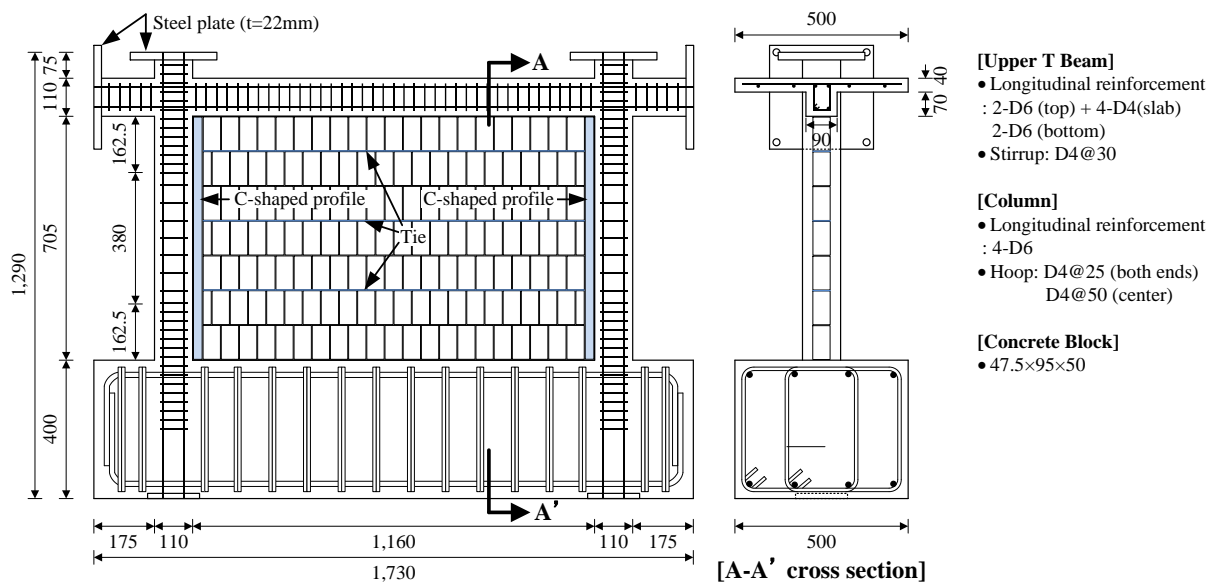
Figure 2. Details of specimen with the tie system (unit: mm)

(a) C-shaped profile
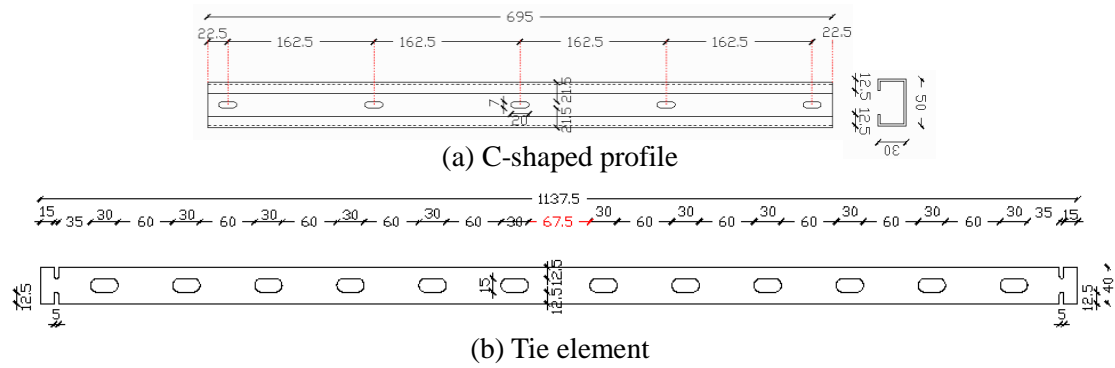
(b) Tie element

Figure 3. Drawings of C-shaped profile and tie element (unit: mm)

(a) Fabrication of tie system   (b) C-shaped profile   (c) C-shaped profile–tie element connection
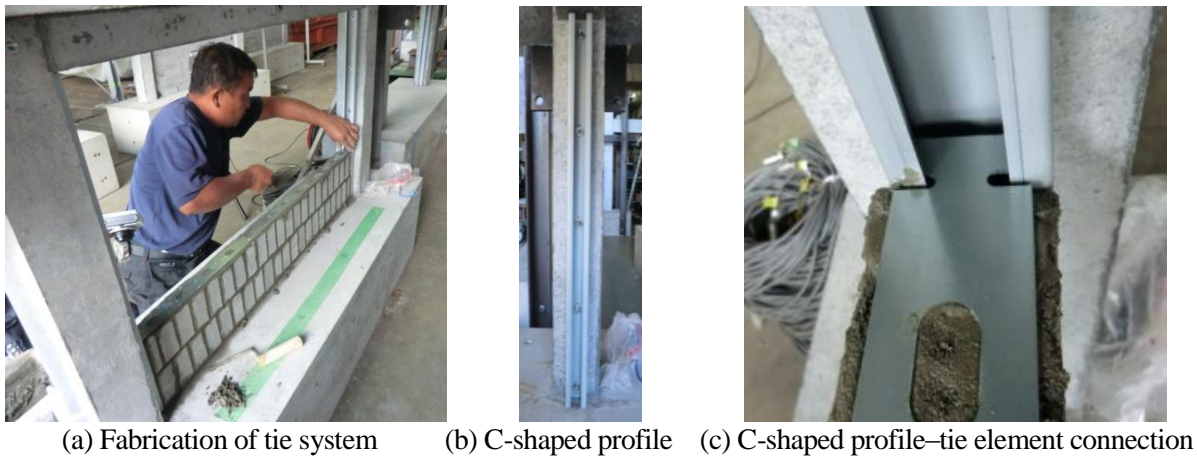
Photo 1. Installation of the tie system

Figure 2 shows the details of the tie system specimen, and Figure 3 and Photo 1 show the drawings and the installation of the tie system, respectively. As shown in Figure 2 and Photo 1, the tie system specimen has two C-shaped profiles anchored to both columns and three tie elements on the second, fourth and sixth layers of the wall.

The masonry unit was also scaled by 1/4. In this study, the concrete block (CB) unit was employed instead of the hollow clay brick generally used in Turkey. However, the cement-to-sand ratio was adjusted so that the strength and stiffness of three layered CB prism specimens corresponded to those of the full scale hollow clay brick whose details were described by Gülkan et al. (2015). The CB units were vertically stacked, as shown in Figure 2 and Photo 1, which was often found in Turkey.

It should be noted that the main objectives of this study are to identify the in-plane effectiveness of the tie system, as mentioned earlier, and to investigate the influence of in-plane damage on out-of-plane failure because infill walls generally suffer some in-plane damage prior to out-of-plane damage. For achieving both purposes, in-plane static cyclic tests were first performed before out-of-plane shaking table tests. In the following chapters, both test results were described, respectively.

IN-PLANE STATIC CYCLIC TESTS

In the in-plane static cyclic tests, the URM wall and tie system specimens were loaded until the peak drift angle of R=2.0%, which is the safety limit of RC buildings specified in the Turkish Guidelines (Turkish Standards Institution (2000)). The details of the in-plane static cyclic tests are provided by the reference (Choi, H. et al. (2015)). Figures 4 through 6 show the lateral load-drift angle relationships, the equivalent damping ratios and the final crack patterns of both specimens, respectively. The equivalent damping ratios of both specimens shown in Figure 5 were similar regardless of the presence or absence of the tie system, although the shear strengths of each drift angle in the tie system specimen were slightly lower than those in the URM wall specimen, as shown in Figure 4. On the other hand, the crack patterns in the walls of both

specimens were quite different, as shown in Figure 6. The corner crushing regions and diagonal crack developments in the wall of the tie system specimen were obviously less extensive than those of the URM wall specimen. These results implied that the tie system is able to ensure the stability of infill walls under an in-plane force.

(a) URM wall specimen (b) Tie system specimen
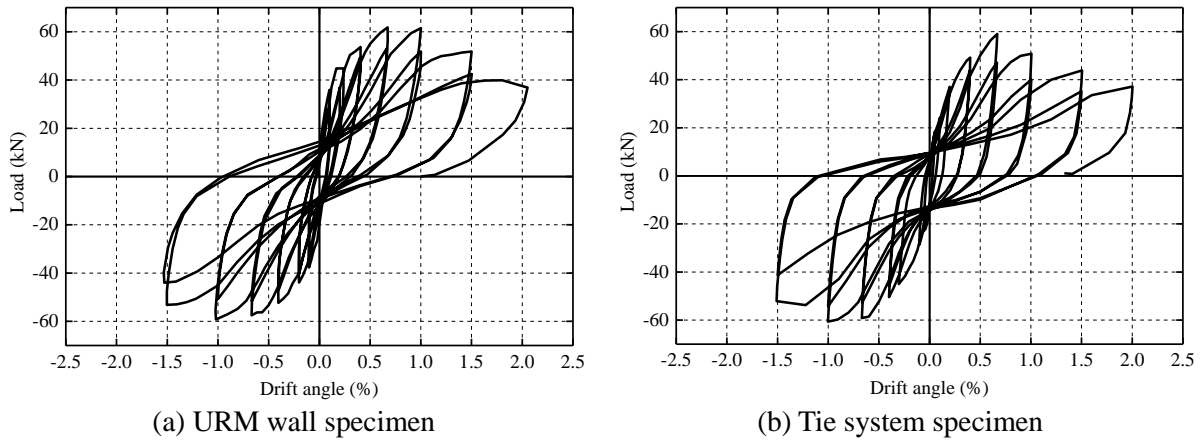
Figure 4. Load vs. drift angle of each specimen
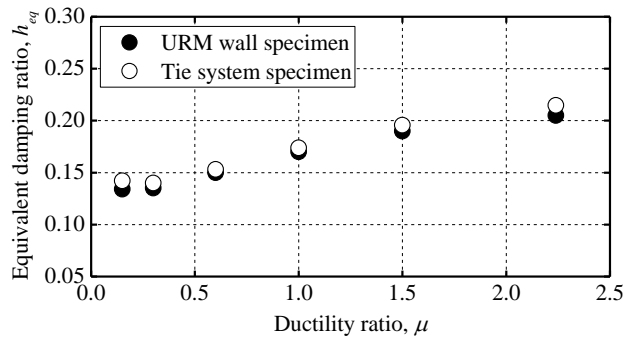
Figure 5. Equivalent damping ratios of each specimen

(a) URM wall specimen (b) Tie system specimen
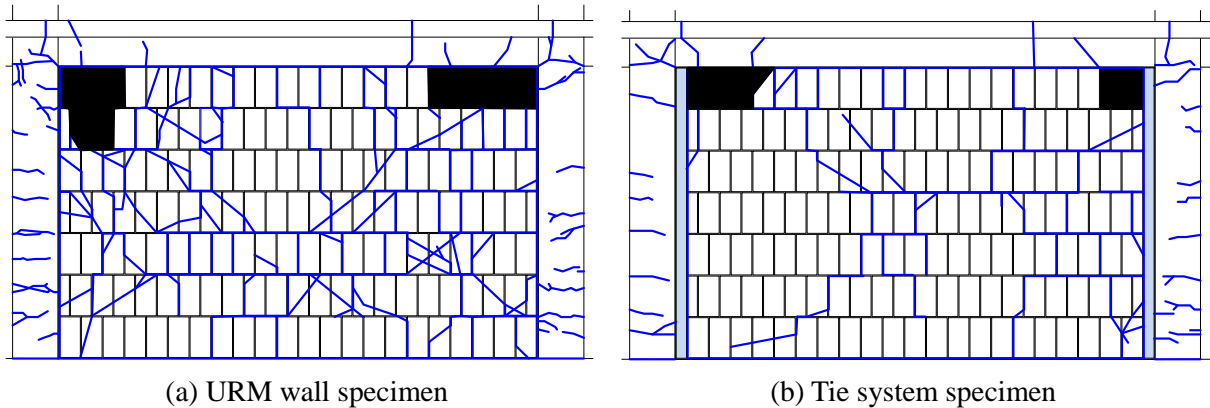
Figure 6. Crack patterns at the peak drift angle of 2.0% during in-plane loadings

OUT-OF-PLANE SHAKING TABLE TESTS

Using the specimens having the in-plane damage stated in the previous chapter, shaking table tests were then performed to investigate out-of-plane behaviors of the walls with or without the tie system. In this study, the wall behavior in the fifth story, which is the top story of the reference building, was focused, because infill walls in the upper story are more vulnerable to the out-of-plane excitation than those in the lower story. The details of the tests were described as below.

Test Setup and Measurement System

Figure 7 and Photo 2 show the test setup and measurement system. Both specimens were tightly connected through steel beams, as shown in Figure 7 and Photo 2, and dynamic excitations were applied simultaneously to both specimens. As for the measurement system, the relative lateral displacement of the overall frame between an upper beam and a lower stub, and the relative lateral displacement of the CB unit at its center of each layer, except for the first layer of both walls, were measured using laser transducers. To measure the response acceleration of the overall frame and both walls, accelerometers were attached on the connecting steel beam and on the center of second, fourth and sixth layers in both walls.
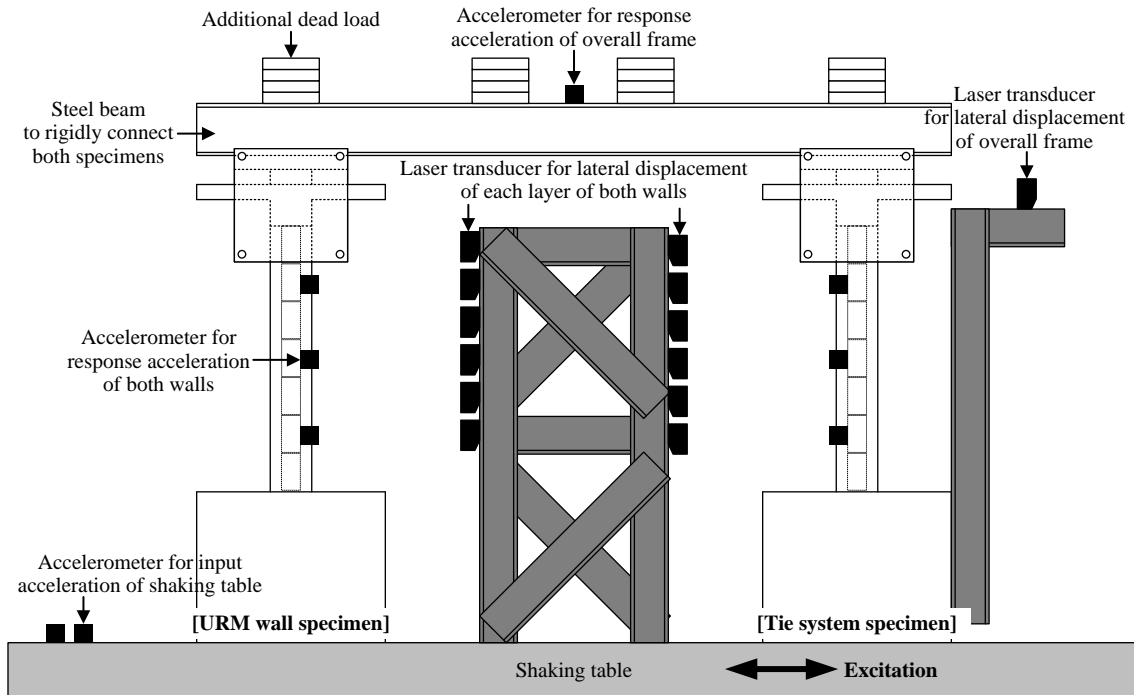
Figure 7. Shaking table test setup and measurement system
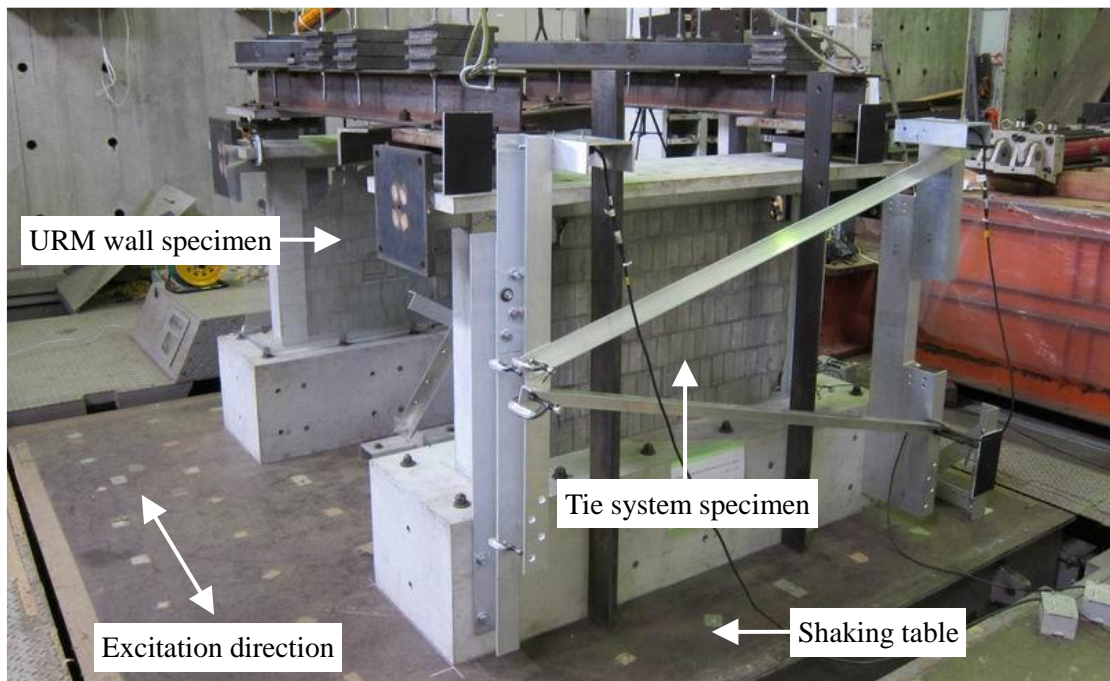
Photo 2. Shaking table test setup

Test Program

The EW component of acceleration recorded during Erzincan earthquake (1992) was employed for the input data of shaking table tests, and the time interval and amplification of the acceleration data were scaled according to the following manner with the similitude requirements. Figures 8 and 9 show the original and modified acceleration data and their acceleration response spectra, respectively.

(1) To obtain the response acceleration data at the fifth floor of the reference building, the elastic response analysis of the reference building, numerically modeled by five-degree of freedom model, was performed using the original acceleration wave (Figure 8 (a)). The obtained response acceleration wave and its acceleration response spectrum are shown in Figures 8(b) and 9(b), respectively. As shown in Figure 9(b), the predominant period of the five-story reference building was approximately 0.60s.

(2) Since each specimen is a single-story model and hence its predominant period is much shorter than that of five-story building, the time interval of the response acceleration data obtained in (1) was decreased by multiplying a reduction factor to emulate the input acceleration of the fifth floor suitable for the single-story specimen. If the single-story specimen is intact, the reduction factor of the time interval is determined as the ratio of the elastic periods of the single-story specimen to the five-story building (=0.19s/0.60s). Since the small scale specimens used in the out-of-plane tests, however, had already suffered some damage during the in-plane static cyclic tests, as mentioned earlier, the period of the single-story specimen even in the out-of-plane direction were also elongated according to its damage. In this study, the predominant period in the out-of-plane direction of a damaged single-story building was estimated 0.31s considering (a) measured period of small scale specimen, 0.11s, after the in-plane loading, and (b) scale similitude requirement $2\sqrt{2}$ which will appear in the subsequent discussions, i.e., $0.11s*2\sqrt{2}$ =0.31s. It should be note that the value of 0.11s was consistent with the period (T_{Ky}) at yielding point shown in Figure 10. Consequently, the reduction factor of the time interval between the single and five-story building was employed as 0.52 (=0.31s/0.60s (=(0.19s/0.60s)*(0.31s/0.19s))), and the obtained response acceleration wave and its spectrum are shown in Figures 8(c) and 9(c), respectively.

(3) Next, the time interval of the acceleration data obtained in (2) was further increased so that the wall behavior in the inelastic range could be properly investigated. Herein, the target deformation δ_p was set to be $2\delta_y$ (δ_y: yield drift), and the factor of the time interval was determined as $\sqrt{2}$, as shown in Figure 10. The acceleration wave and its spectrum obtained by the procedures above are shown in Figures 8(d) and 9(d), respectively.

(4) The input acceleration wave for the 1/4-scale specimen was finally obtained using the similitude requirement so that the shear stresses in the small scale specimen could reproduce that of full scale (Equation (1-1)). Consequently, the target acceleration amplitude was calculated by multiplying the acceleration obtained in (3) and the factor of 2 found in Equation (2-1) derived from Equations (1-1) through (1-4), and the time interval was compressed by the factor of $1/2\sqrt{2}$ found in Equation (3) obtained from Equations (2-1) through (2-3). It should be noted that the density of the small scale CB unit was found to be two times that of the full scale hollow clay brick unit, generally used in Turkey; that is, $\rho_S=2\rho_F$, and Equation (1-4) was obtained. Considering the main objective of this study is to discuss the out-of-plane behavior of masonry unit, this similitude requirement rule was applied to the whole specimen. The data obtained by the procedures above was then regarded as a standard wave for the small scale specimens, as shown in Figure 8(e), and its acceleration response spectrum is shown in Figure 9(e).
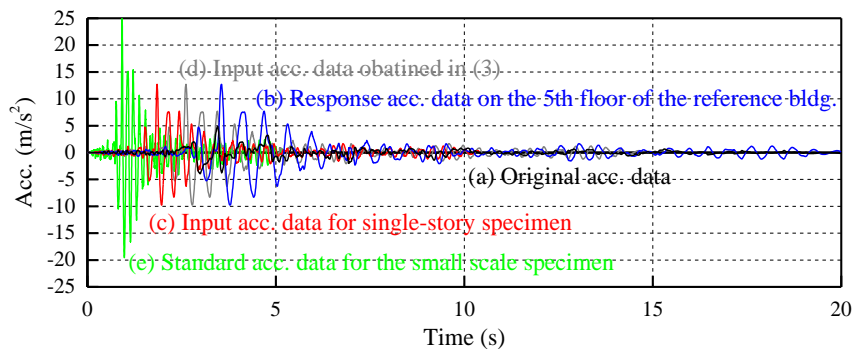
Figure 8. Original and modified acceleration data
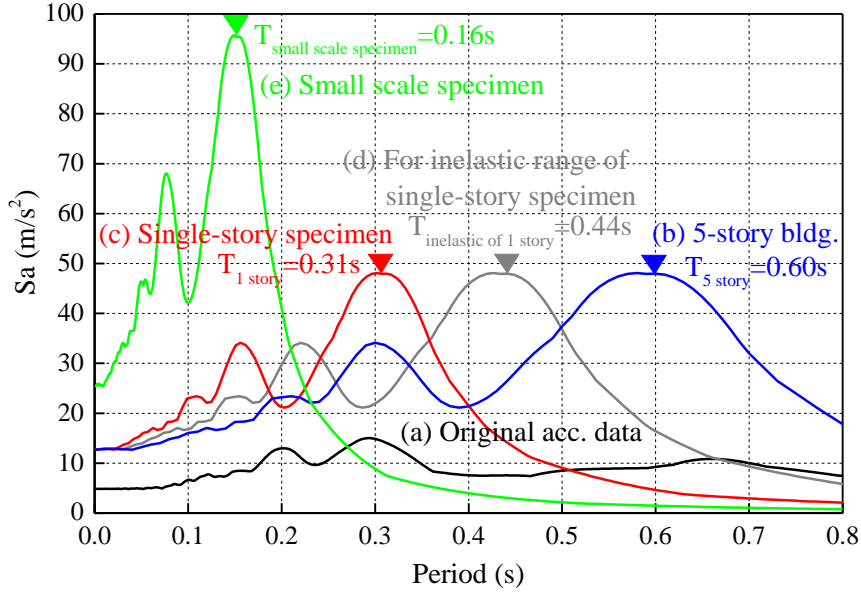
Figure 9. Acceleration response spectra of original and modified acceleration data
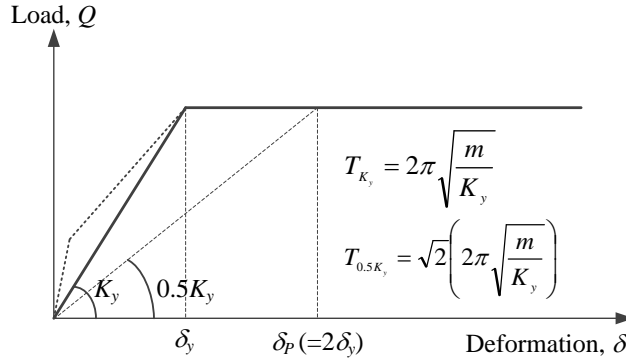
Figure 10. Periods according to the stiffness and ductility ratio in the out-of-plane direction

$$\tau_S = \tau_F \tag{1-1}$$

$$\rightarrow \frac{m_S \cdot \ddot{x}_S}{A_S} = \frac{m_F \cdot \ddot{x}_F}{A_F} \tag{1-2}$$

$$\rightarrow \frac{V_S \cdot \rho_S / g \cdot \ddot{x}_S}{A_S} = \frac{V_F \cdot \rho_F / g \cdot \ddot{x}_F}{A_F} \tag{1-3}$$

$$\rightarrow \frac{\alpha^3 \cdot V_F \cdot 2\rho_F / g \cdot \ddot{x}_S}{\alpha^2 \cdot A_F} = \frac{V_F \cdot \rho_F / g \cdot \ddot{x}_F}{A_F} \tag{1-4}$$

$$\ddot{x}_S = 2 \cdot \ddot{x}_F \tag{2-1}$$

$$\rightarrow \frac{L_S}{T_S^2} = 2 \cdot \frac{L_F}{T_F^2} \tag{2-2}$$

$$\rightarrow \frac{\alpha \cdot L_F}{T_S^2} = 2 \cdot \frac{L_F}{T_F^2} \tag{2-3}$$

$$T_S = \frac{1}{2\sqrt{2}} T_F \tag{3}$$

where τ_S and τ_F are the shear stresses of the small and full scale specimens, respectively; m_S and m_F are the masses of the small and full scale specimens, respectively; $\ddot{x}_s$ and $\ddot{x}_F$ are the accelerations of the

small and full scale specimens, respectively; A_S and A_F are the areas of the small and full scale specimens, respectively; V_S and V_F are the volumes of the small and full scale specimens, respectively; ρ_S and ρ_F are the densities of the small and full scale specimens, respectively; g is the acceleration of gravity; α is the scale ratio (=1/4); L_S and L_F are the lengths of the small and full scale specimens, respectively; T_S and T_F are the predominant periods of the small and full scale specimens, respectively.

In this study, the target peak acceleration was scaled to each excitation level; that is, the target peak acceleration of Run1 through Run6 were set to be 2.6 m/s² (10%), 6.4 m/s² (25%), 12.8 m/s² (50%), 19.1 m/s² (75%), 25.5 m/s² (100%) and 30.6 m/s² (120%), respectively, as summarized in Table 1. However, the achieved peak acceleration value recorded on shaking table had slight discrepancies, and they were 2.2 m/s² (9%), 5.5 m/s² (21%), 10.7 m/s² (42%), 18.0 m/s² (71%), 22.4 m/s² (88%) and 25.5 m/s² (100%). Since the out-of-plane failure in both walls did not occur until Run6, Run7 was set to have the same peak acceleration value but different time interval from Run6. To increase the response displacement of the overall frame, the time interval at Run7 was set as 1.3 times of preceded runs, as shown in Table 1.

Table 1. Loading protocol

	Target acceleration level	Maximum acceleration (m/s²)	Achieved input acceleration level	Maximum acceleration (m/s²)
Run1	10%	2.6	9%	2.2
Run2	25%	6.4	21%	5.5
Run3	50%	12.8	42%	10.7
Run4	75%	19.1	71%	18.0
Run5	100%	25.5	88%	22.4
Run6	120%	30.6	100%	25.5
Run7	-	-	100% (1.3 times of time interval)	25.3

Experimental Results

Response Acceleration – Response Displacement Relationships of the Overall Frame
Figure 11 shows the response acceleration – response displacement relationships of the overall frame in each run. The maximum response points in each run from the experimental results and calculated yield strength of the overall frame are also plotted in the figure. The maximum responses were defined as the points which recorded the maximum displacement just before the unloading started during the largest hysteresis loop. As shown in Figure 11, the maximum displacements of both directions were approximately the same until Run 4 (71%), while they were larger in the negative direction than in the positive direction after Run 5 (88%). This result was caused by the employed acceleration data, in which the maximum acceleration of the positive direction was greater than that of the negative direction, as shown in Figure 8(e). The strengths at maximum response points after yielding were approximately consistent with the calculated yield strength.

Figure 12 compares the Sa – Sd curve computed to the recorded acceleration and the capacity curve contributed by both specimens. The maximum response points shown in Figure 11 are also plotted in the figure. As shown in Figure 12, the intersection points between the response and capacity curves are supposed to be the maximum responses of the specimen in each run. The estimated intersection points reasonably agreed with the maximum responses obtained from the tests during the elastic range (until Run 3 (42%)). For Run 4 (71%) with roughly the same maximum displacements in the positive and negative directions (Figure 11), the intersection point was larger than the recorded response. However, the intersection point could be closer to the test result if a higher hysteresis damping was properly considered in calculating the response curve. In contrast, after Run 6 (100%) with larger maximum displacement in the negative direction, the intersection point was smaller than the recorded response. In the case with one-sided larger maximum displacement in either negative or positive direction, a rational hysteresis damping might be required to predict the maximum responses.
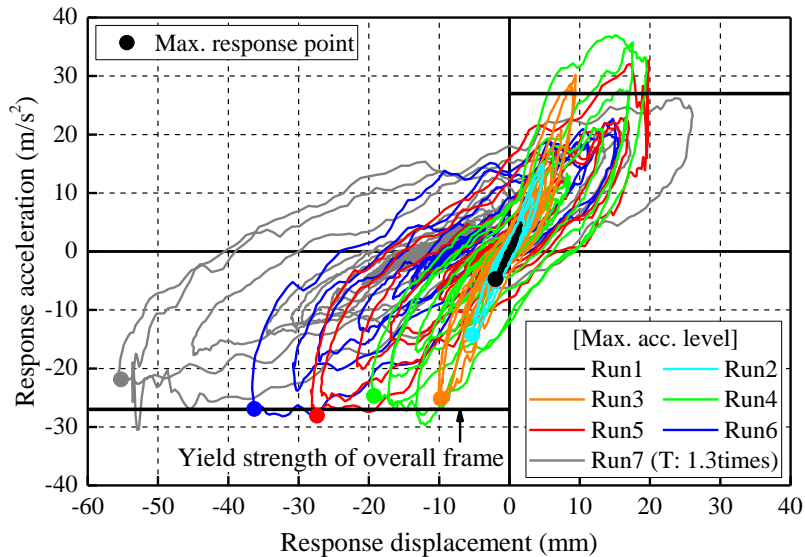
Figure 11. Response acceleration vs. response displacement in each run
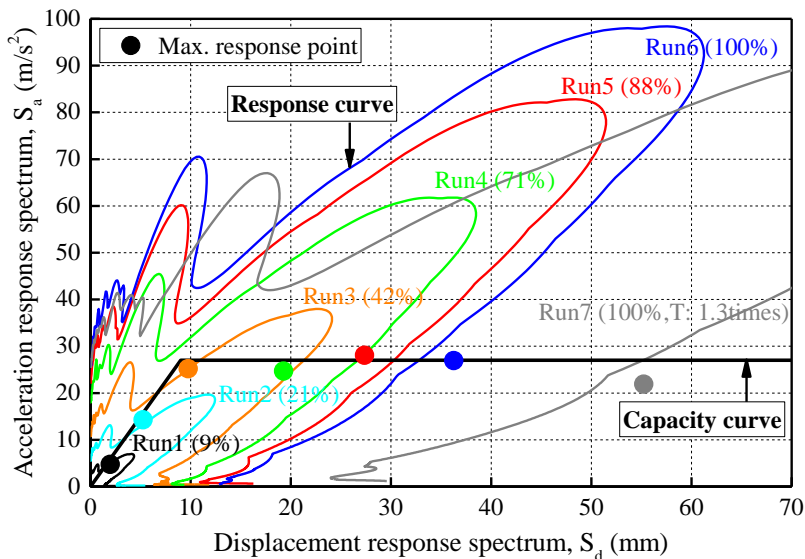
Figure 12. Intersection of response and capacity curves vs. maximum response points

Deformation and Acceleration Distributions of the Infill walls

Figure 13 shows the distributions of the lateral deformation in both walls including the specimen's top displacement (plotted at 700 mm high in the vertical axis of the figure), when the deformation of fifth layer of the infill recorded the maximum value. Since the laser transducer data for the sixth and seventh layers were not measured properly during the test, the accelerometer data on the sixth layer were used to calculate its lateral deformation, which was obtained from a double integration of the acceleration. The integration method applied to this study was briefly summarized in Appendix. As shown in Figure 13, the deformations of both walls were distributed linearly toward the top displacements of the specimen throughout the whole excitations.

Figure 14 shows the acceleration distributions in each run of both walls when the maximum acceleration was recorded among three accelerometers. As shown in the figure, the acceleration distributions of both walls showed approximately linear profile.

Figure 15 shows the ratios of the maximum deformation and the maximum acceleration of the tie system wall to those of the URM wall in each run. As can be seen in the figure, much higher acceleration was imposed in the tie system wall than in the URM wall, although the lateral deformations in both walls were similar. These results could be attributed to the less damage to the tie

system wall during the in-plane static cyclic loading and to the effect of reducing the out-of-plane response of the wall due to the proposed reinforcing tie system.

(a) URM wall   (b) Tie system wall
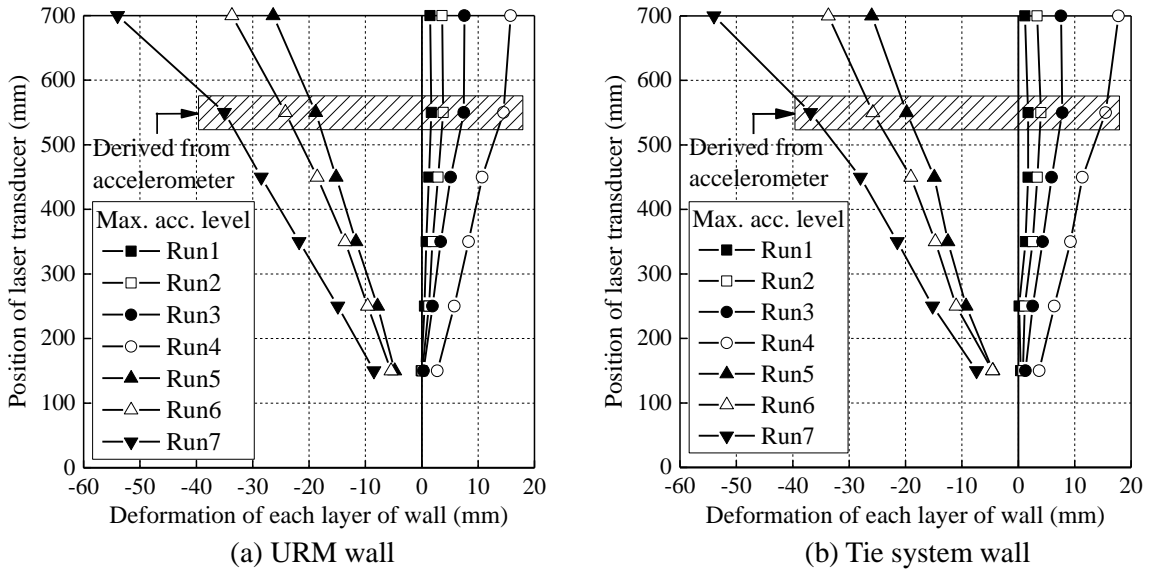
Figure 13. Deformation distributions of the CB walls

(a) URM wall   (b) Tie system wall
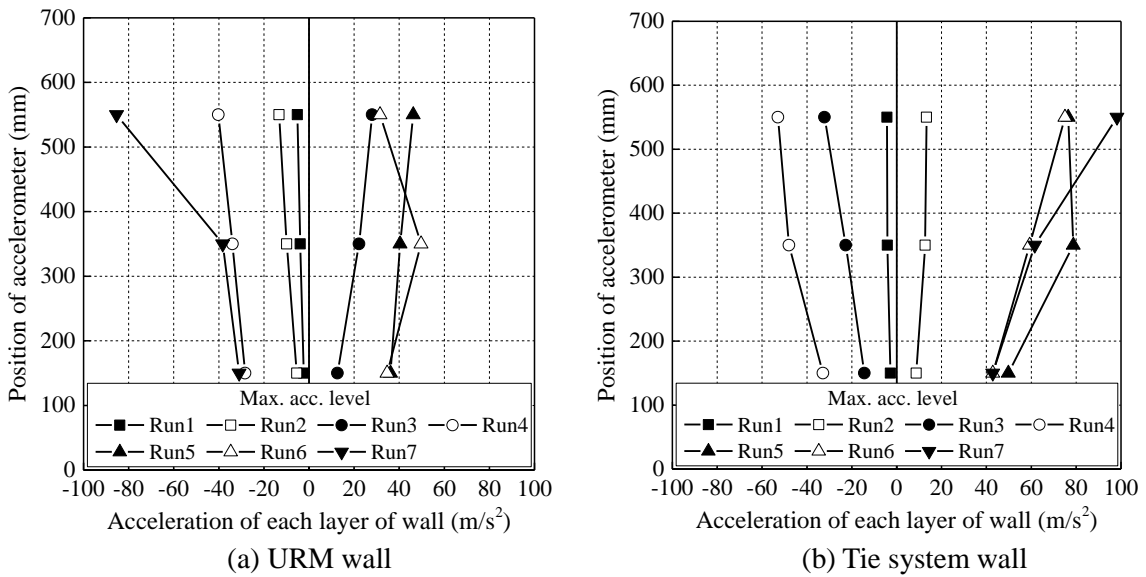
Figure 14. Acceleration distributions in the CB walls
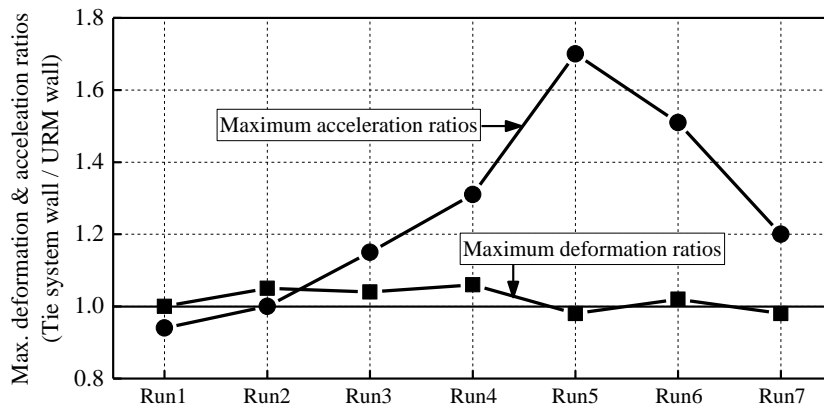
Figure 15. Maximum deformation and maximum acceleration ratios in both walls

Figure 16 shows the damage to CB walls in both specimens after final excitation Run7. The spalling ratios of CB walls with respect to each run, which are defined as the spalled to the whole surface area of the infill, are shown in Figure 17. As shown in the figures, the infill damage to the tie system specimen was almost the same as that before the out-of-plane excitation shown in Figure 6, while that of the URM wall specimen considerably increased by five times.

From the experimental investigation by the in-plane static cyclic tests and out-of-plane shaking table tests, the tie system proposed in this study were found to provide higher stability with the infill walls under both in- and out-of-plane forces; therefore, it was found to provide a reliable contribution of the infill to the lateral load resistance of the overall frame.

(a) URM wall specimen   (b) Tie system specimen
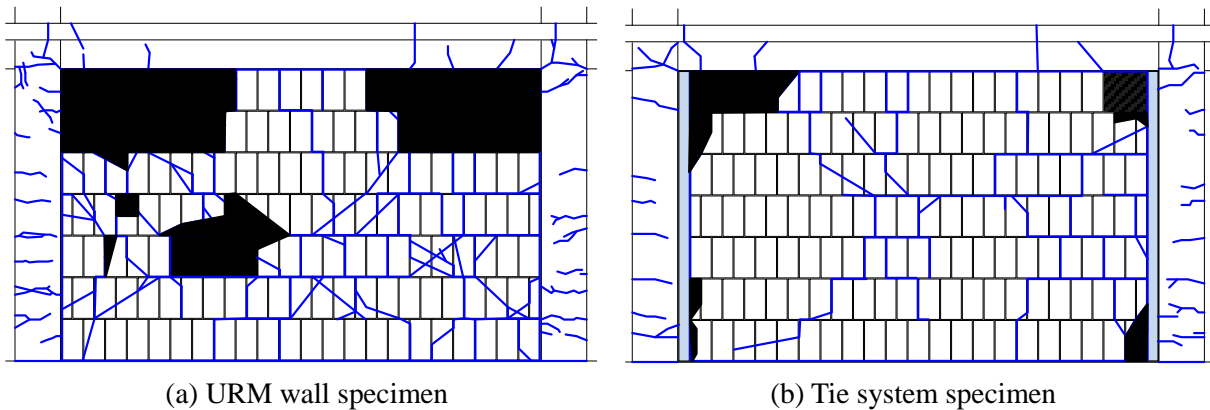
Figure 16. Damage to CB walls after final out-of-plane excitation Run7
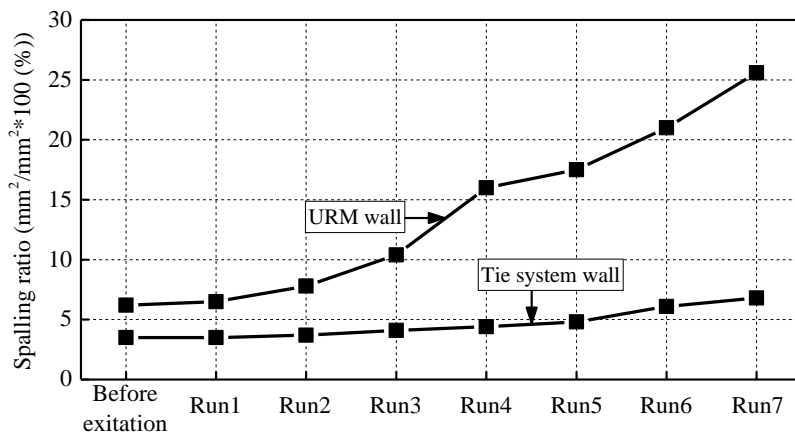
Figure 17. Spalling ratios of CB walls with respect to each excitation

CONCLUSIONS

The current paper reported the experimental results of the in-plane static cyclic tests and out-of-plane shaking table tests on Turkish RC frames with infill walls. From the experiments, the in-plane and out-of-plane behaviors of URM infill walls were investigated, and the effectiveness of the proposed tie system was discussed. Consequently, the following major findings were obtained:

(1) The in-plane seismic capacity of each specimen was similar regardless of the presence or absence of the tie system. However, the damage such as corner crushing regions and crack developments in the wall of the tie system specimen was obviously less extensive than those of the URM wall specimen. These results implied that the tie system is expected to ensure the stability of infill walls under an in-plane force.

(2) From the shaking table test results, the maximum response points after yielding reasonably agreed with the calculated yield strength. In addition, the intersection points obtained from the response and capacity curves were approximately consistent with the recorded response points.

(3) Much higher acceleration was imposed in the tie system wall than in the URM wall, although the lateral deformations in both walls were similar. Moreover, the infill damage to the tie system specimen was almost the same as that before the out-of-plane excitation, while that of the URM wall specimen considerably increased by five times. These results could be attributed to the less damage to the tie system wall during the in-plane static cyclic loading and to the effect of reducing the out-of-plane response of the wall due to the proposed reinforcing tie system.

(4) From the test results, the tie system proposed in this study were found to provide higher stability with the infill walls under both in- and out-of-plane forces, and the system provided a reliable contribution of the infill to the lateral load resistance of the overall frame.

APPENDIX: DOUBLE INTEGRAION METHOD OF ACCELERATION RECORD APPLIED IN THIS STUDY

In general, when an acceleration record is integrated twice to obtain the displacement data, the resultant displacement tends to be divergent due to the baseline deviation of accelerometers and noise of a measurement system. To prevent such divergence, the double integration method proposed by Iwan et al. (1985) was employed in this study. The method was briefly explained using the acceleration and displacement data measured at the fourth layer of the infill wall, as follows:

(i) First, an acceleration record was divided into three sections: the first section is the range before the major excitation which has a peak acceleration higher than 5 m/s^2 herein ((1) in Figure A1(a)), the second section is the major excitation range ((2) in Figure A1(a)), and the third section is the remaining range ((3) in Figure A1(a)), respectively.

(ii) Second, since the initial acceleration should be zero in average but some noise signal is generally recorded, such signal error was corrected by the horizontal axis offset for the whole range (1) through (3). The offset value was calculated form the mean value of the acceleration data in Section (1) (red line in Figure A1(a)).

(iii) Third, the velocity wave (red line in Figure A1(b)) was calculated by integrating the corrected acceleration data obtained in (ii).

(iv) Fourth, assuming the baselines of velocity in sections (2) and (3) were linear functions (Figure A1(b)), respectively, the acceleration data of both sections were corrected so that the average velocity with respect to the assumed baseline should be zero (blue line in Figure A1(b)).

(v) Finally, the displacement (red line in Figure A1(c)) was obtained by integrating the corrected velocity data obtained in (iv). As shown in Figure A1(c), the calculated displacement wave agreed well with the measured displacement throughout the whole range.
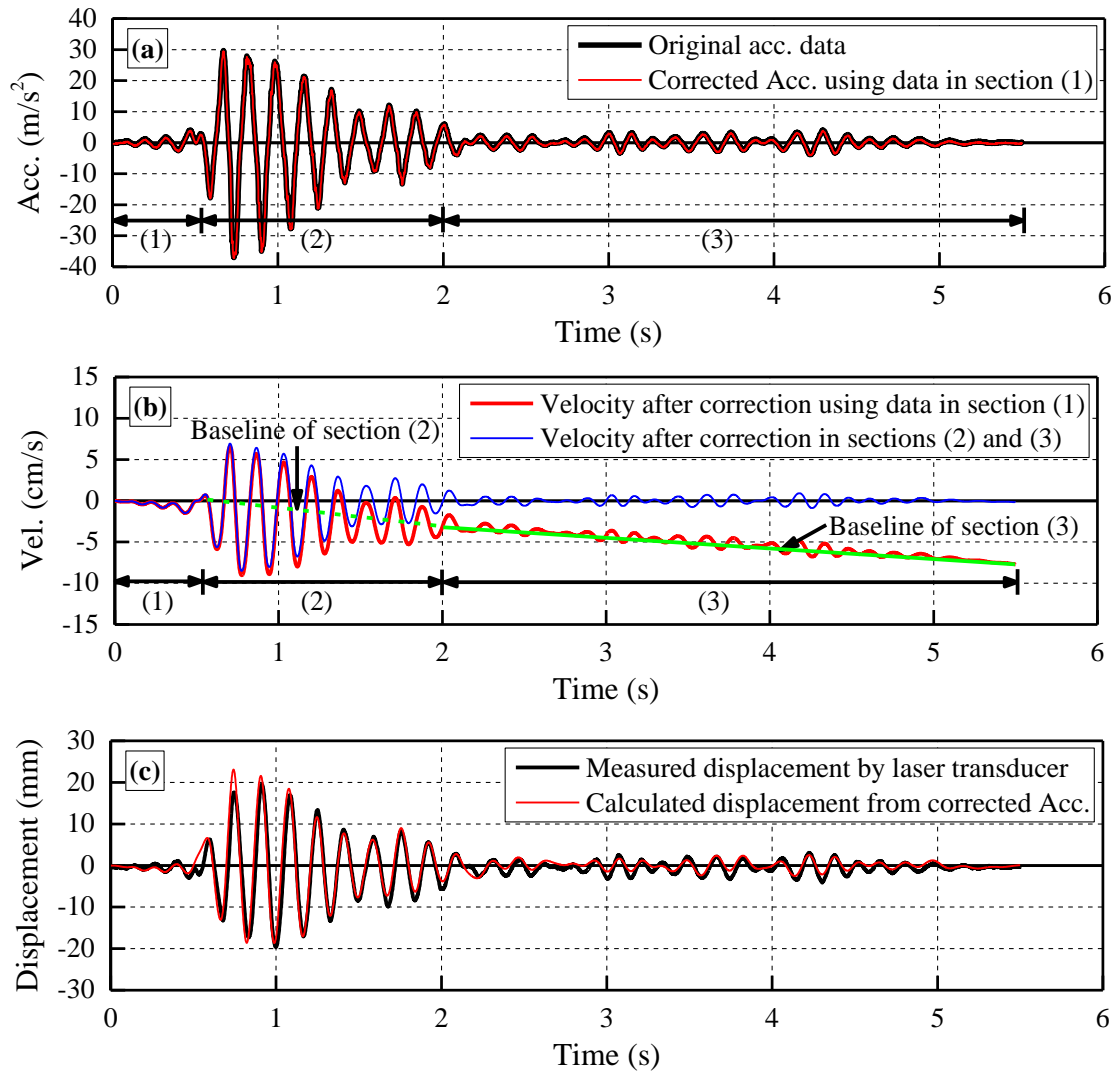
Figure A1. Double integration method employed in this study

REFERENCES

Jin, K., Choi, H. and Nakano, Y. (2016). "Experimental Study on lateral Strength Evaluation of Unreinforced Masonry-Infilled RC Frame". *Earthquake Spectra*, DOI: http://dx.doi.org/10.1193/ 100714EQS152M.

Gülkan P.B., Ninici H., Sucuoğlu A., Taghipour O., Demirel S., Tanışer O., Güneş M., Ismail E., Fehling Y., Nakano Y., Sanada Y. and Choi H. (2015). "An Innovative Tie System for Improving the Monolithic Behavior of Masonry In-filled Reinforced Concrete Frames (INFILTIE)", *3rd Turkish National Conference on Earthquake Engineering and Seismology*.

Turkish Standards Institution. (2000). "Requirements for Design and Construction of Reinforced Concrete Structures", TS500.

Choi, H., Paul, D., Suzuki, T., Matsukawa, K., Sanada, Y. and Nakano, Y. (2015). "Seismic Capacity Evaluation of URM Infill Built in RC Frame, *Summaries of Technical Papers of Annual Meeting, Architectural Institute of Japan (AIJ)*, Vol.IV, pp.777-782.

Iwan, W.D. et al. (1985). "Some Observations on Strong-motion Earthquake Measurement using a Digital Accelerograph". *Bulletin of the Seismological Society of America*, Vol.75, pp.1255-1246.